

Evaluation of fluconazole-loaded nanocellulose-reinforced xanthan gum film for drug delivery applications

Vipin JAIN¹, Rimpay PAHWA², Rashmi SHARMA¹, Munish AHUJA^{1*}

¹ Drug Delivery Research Laboratory, Department of Pharmaceutical Sciences, Guru Jambheshwar University of Science and Technology, Hisar-125001, Haryana, India

² Amity Institute of Pharmacy, Amity University, Noida-201303, Uttar Pradesh, India

ABSTRACT

The purpose of the present study is to prepare xanthan films reinforced with nanocellulose and to evaluate them for drug delivery applications using fluconazole as the model drug. The preparation of films by solvent casting method was optimized using a central composite design. It was observed that increasing the concentration of nanocellulose and polyethylene glycol 4000 increases the tensile strength and delays the release of fluconazole from xanthan gum films. The optimal formulation was composed of nanocellulose (100 mg), polyethylene glycol 4000 (50 mg), and xanthan gum (100 mg) which exhibited the tensile strength of 4220 mN and 100% release of the drug over 24 h. The film had a fibrous surface. The film released fluconazole by zero-order kinetics by super case II transport mechanism. It can be concluded based on the present study that reinforcement of nanocellulose in xanthan gum films improves their tensile strength and imparts sustained release character.

Keywords: fluconazole, nanocellulose, film, xanthan gum, sustained drug delivery

*Corresponding Author: Munish AHUJA

E-mail: munishahuja17@yahoo.co.in

ORCID:

Vipin JAIN: 0009-0003-8569-5496

Rimpay PAHWA: 0000-0003-2087-1105

Rashmi SHARMA: 0000-0002-9364-9188

Munish AHUJA: 0000-0001-6723-140X

(Received 23 May 2023, Accepted 9 Oct 2023)

INTRODUCTION

Xanthan gum is an extracellular microbial heteropolysaccharide produced by the bacterium *Xanthomonas campestris*. It is composed of dual pentameric units including two glucose units, two mannose units, and a glucuronic acid in the ratio of 2.8:2.0:2.0^{1,2}. Xanthan gum is a high molecular weight long-chain polysaccharide with functional groups³⁻⁵. Due to its special rheological properties, it has been widely used as stabilizing, suspending, thickening, and emulsifying agent in various industries. Xanthan gum is also used in film formation with appropriate gloss⁶. Various researchers have focused on preparing the xanthan gum-based composite films using sodium alginate, carrageenan, gum Arabic, polyvinyl alcohol, pullulan, and hydroxypropyl methylcellulose⁶⁻⁹. Xanthan gum-based film formulations have been employed for a number of applications such as mucoadhesive buccal film^{10,11}, buccal patch², orodispersible film¹², mouth dissolving films¹³, transdermal patch¹⁴, dermal dressings¹⁵, and as antibacterial film¹.

Nanocellulose is defined as the nano-scaled cellulosic material having a diameter in the range of 1-100 nm. Depending upon the method of synthesis, source, dimension, composition, and properties, the nanocellulose is referred to as cellulose nanofibers, bacterial cellulose, and cellulose nanocrystals^{16,17}. A great number of reported articles show that nanocellulose-reinforced polymeric composite films have a lot of properties like design flexibility, tolerability, high mechanical strength of the film, and easy processing which makes these composites highly usable in food packaging, automotive, biotechnological, and pharmaceutical industries¹⁸⁻²³. As per earlier reports nanocellulose, as reinforcing agent in the starch-based composites provided the high aspect ratio, improved mechanical properties, and high Young's modulus^{24,25}. Most of the studies of nanocellulose reinforced chitosan films, emphasized on enhancement of mechanical properties and preservation of the antibacterial property of the films^{26,27}. It is also reported that when alginate-based films were reinforced with nanocellulose, the tensile strength, and thermal stability were increased while water vapor permeability was decreased²⁸. Gelatin films with nanocellulose reinforcement showed an improvement in mechanical properties as well as oxygen gas barrier properties²⁹. The incorporation of nanocellulose in polyvinyl alcohol-based composite films much improved the barrier properties and mechanical strength of the films^{30,31}. In one of the research projects, nanocellulose reinforcement in polyvinyl alcohol film exhibited outstanding UV-blocking property³². Some crystalline nanocellulose products have also shown sustained drug release behaviour¹⁶. Xanthan gum and nanocellulose are reported to possess mucoadhesive properties^{10,20,23}.

Nanocellulose-reinforced xanthan gum film may be potentially useful as food packaging material, UV-blocking film, antimicrobial film, transdermal patch, mucoadhesive buccal or vaginal film, buccal patch, and dermal dressing. To the best of our comprehension, no report has been made on the nanocellulose-reinforced xanthan gum film. Therefore, the purpose of this study was to observe the changes in the physicochemical characteristics and release behaviour of xanthan gum by reinforcing with nanocellulose using fluconazole as the model drug. The two-factor three-level central composite experimental design was employed to obtain the optimized batch of film. The prepared polymeric films were characterized further utilizing many characterization techniques such as thickness, tensile strength, surface pH, swelling capability, Fourier transform-infrared spectroscopy (FT-IR), X-ray diffraction (XRD), scanning electron microscopy (SEM), and *in vitro* drug release study for drug delivery applications.

METHODOLOGY

Materials

Rice nanocellulose (α -cellulose = 91.78%, mol. wt. = 1.16×10^7 g/mol, particle size = 441.7 nm) was isolated from rice straw as per the previously reported literature and used for the present study³³. Fluconazole was received as a gift sample from Hetero Drugs Ltd. (Hyderabad, India). Xanthan gum, sodium hydroxide, and glacial acetic acid were purchased from Sisco Research Laboratories Pvt. Ltd. (Maharashtra, India). Sodium hypochlorite was obtained from Loba Chemie Pvt. Ltd. (Mumbai, India). Polyethylene glycol 4000 (PEG) was procured from Thomas Baker (Chemicals) Pvt. Ltd. (Mumbai, India). Disodium hydrogen orthophosphate and sodium dihydrogen orthophosphate were purchased from High Purity Laboratory Chemicals Pvt. Ltd. (Mumbai, India). Glycerine and oxalic acid were procured from Central Drug House Pvt. Ltd. (Delhi, India).

Extraction of rice nanocellulose

Initially, rice straws were collected from agricultural land and washed properly using water to remove dirt and other impurities. The extraction process of nanocellulose consists of three steps. In the first step, 10 g of rice straws were taken and cut into small pieces. The pieces of straws were placed into a 1000 mL beaker and then treated with sodium hydroxide solution (5% w/v) for 6 h under mechanical stirring. The slurry was filtered and washed with distilled water. The washing step was repeated five times for the complete removal of lignin and hemicellulose. In the next step, the rice pulp was treated with 10 mL of sodium hypochlorite and 1 mL of glacial acetic acid under mechanical stirring for 6 h, followed by washing with distilled water. This step was repeated till the pulp be-

came white in color. In the last step, the obtained white pulp was treated with 5 g of oxalic acid and stirred continuously for the time interval of 6 h. Thus, the obtained nanocellulose was washed with distilled water for 2 to 3 times to remove any other chemical impurities and subjected to deep freezing at -40 °C for drying. The dried nanocellulose was stored in an airtight container for further use³³.

Preparation of fluconazole-loaded xanthan-nanocellulose film

The fluconazole-loaded polymeric film was prepared by employing the solvent casting method. Initially, a definite amount of xanthan gum was weighed and swelled in distilled water for 24 h. In an aqueous solution of fluconazole, a pre-weighed quantity of nanocellulose and PEG was added and stirred up to 4 h. Then, the nanocellulose dispersion was mixed with swelled xanthan gum and stirred continuously for 2 h. The prepared fluconazole-loaded xanthan-nanocellulose solution was poured into a Petri dish and dried in a hot air oven at 50 °C for 36 h. The obtained fluconazole-loaded xanthan-nanocellulose film (XNF) was stored in a desiccator for further characterization and evaluation. For comparative evaluation, native fluconazole-loaded xanthan film (XF) and fluconazole-loaded nanocellulose film (NF) were also prepared.

Experimental design

A two-factor, three-level central composite experimental design was applied to examine the effect of different parameters in preparation for appropriate formulation by using Design Expert Software (trial version 11.0.0, Stat-Ease Inc., Minneapolis, MN). The amount of nanocellulose (25-100 mg, X_1) and amount of PEG (15-50 mg, X_2) were selected as independent variables whereas, tensile strength (Y_1) and *in vitro* release (Y_2) were taken as response variables. Thirteen batches were prepared as per the software and entries of independent variables were coded as low (-1), medium (0), and high (+1). Analysis of variance (ANOVA) was used to determine the R^2 value (coefficient of determination), adjusted R^2 value, predicted R^2 value, adequate precision, coefficient of variance, and lack of fit values.

Characterizations of film

Physicochemical properties

Percent moisture content

To calculate the percentage of moisture absorbed by the formulation, the precise weight of a dried film was measured (W_0). The pre-weighed film was introduced into a chamber with a constant relative humidity of 75% at a temperature of 40 °C, where it remained for a period of 72 h³⁴. Then the weight of the film was calculated again (W_1). Then, the percentage of moisture content was determined using the following equation 1:

$$\% \text{ Moisture content} = \frac{W_t - W_o}{W_o} \times 100 \quad (1)$$

Average weight

Three pieces of the film (2 cm × 2 cm) were cut and weighed individually using a digital weighing balance. The average weight was calculated and expressed as mean ± standard deviation.

Film thickness

The thickness of the film is the important parameter that ensures the content uniformity of the prepared film. The thickness was measured at different edges by using Vernier Caliper (YAMAYO® Classic, Japan) and the average thickness was calculated³⁵.

Tensile strength

The tensile strength measures the maximum force applied to the point at which the film breaks. The film (2×2 cm²) was taken and hung between two clamps attached with a hardness tester (VG-500, Vin Syst Technologies, India), and load or force was applied at the lower end. The force was noted at which the film broke. This test was performed three times for accurate results and an average reading was noted.

Surface pH

The pH of the surface was identified by selecting the random sections of films (1 cm²) and allowing them to swell in 5 mL of distilled water. Then the pH was measured by using a digital pH meter (pH Testr 10, Eutech Instruments, Singapore)³⁶.

Swelling study

The swelling property of XF, NF, and XNF was determined in distilled water, HCl buffer (pH 1.2), and phosphate buffer (pH 6.8)³⁷. The prepared films were cut into small pieces, weighed (W_1), and placed individually into solvent-containing Petri dishes. The weights of swelled films (W_2) were measured at different time intervals by removing excess surface liquid with the help of tissue paper and the swelling percentage was calculated using the following equation 2:

$$\text{Swelling \%} = \frac{W_2 - W_1}{W_1} \times 100 \quad (2)$$

Fourier-Transform Infrared Spectroscopy (FT-IR)

The FT-IR spectra of fluconazole, XF, NF, and XNF were estimated using an FT-IR spectrophotometer (Spectrum Two, PerkinElmer Spectrum®, US) for the detection of the functional groups in the prepared film. The sample was mixed with potassium bromide with the help of a mortar and pestle. The pellet was prepared by direct compression using an IR hydraulic press at the pressure of 50 kg/cm² (IR Hydraulic Press CAP-15T, PCI Analytics, Mumbai, India). The IR spectrum was recorded in the range of 4000-400 cm⁻¹.

X-Ray Diffraction (XRD)

XRD is used to determine the nature of a solid whether it is crystalline, amorphous, or semicrystalline. XRD of fluconazole, XF, NF, and XNF were investigated by using different kinds of radiations (Cu, K α , K β) at room temperature (25 °C) by using an XRD instrument (Miniflex 600, Rigaku Corporation, Tokyo, Japan). The XRD pattern was analyzed at a range of scattering angle 2θ (10° to 80°) at a speed of 2°/min.

Scanning Electron Microscopy (SEM)

SEM was used for the determination of the surface topography and morphology of the film. XNF was coated with gold in a sputter coater (DII-29030SCTR, Smart Coater, JEOL, USA) to suppress the charging effects in an electron microscope. The micrographs of the film were captured at different magnifications (100X, 500X, 5000X, and 10000X) in JSM-7610FPLUS, JEOL, Japan.

Drug content (%)

An accurately weighed amount of film (25 mg) was dissolved in 25 mL of distilled water, followed by filtration. The filtrate was diluted appropriately and the drug content in the filtrate was determined by measuring the absorbance in a UV spectrophotometer at λ_{max} 260 nm³³⁻³⁸.

***In vitro* release study**

The *in vitro* release study of fluconazole was performed by using a paddle-type apparatus (USP Type II). A weighed amount of film (50 mg) was placed at the bottom of beakers separately and covered with wire mesh of stainless steel to avoid film floating at the dissolution surface. A definite amount of phosphate buffer (pH 6.8, 900 mL) was taken as the dissolution medium, and the temperature was maintained at 37 ± 0.5 °C with a dissolution speed of 50 rpm for 24 h. An aliquot of 5 mL was withdrawn at different time intervals and replaced with a fresh dissolution medium to maintain the sink condition. The collected

samples were analyzed using a UV spectrophotometer (USP-II, TDI-o8L, Electrolab, Mumbai, India) at a wavelength of 260 nm, absorbance was noted and the cumulative percentage of drug release was calculated. The release data was fitted into four different drug release kinetic models i.e., zero-order (% cumulative release vs time), first-order [$\log(100 - \% \text{ cumulative release})$ vs time], Higuchi model (% cumulative release vs square root time), and Korsmeyer Peppas model ($\log \% \text{ cumulative release}$ vs $\log \text{ time}$). Further, the obtained equation of the plots and the value of the coefficient of determination (R^2) were compared.

RESULTS and DISCUSSION

Preparation of fluconazole-loaded xanthan-nanocellulose film

In this study, the isolated nanocellulose and xanthan gum were utilized further to develop a sustained-release film of fluconazole. As per the earlier literature, cellulose has been widely used in drug delivery applications due to its various properties like biocompatibility, biodegradability, hydrophilicity, rheological properties, and high mechanical strength. Various cellulose derivatives such as cellulose ethers (methylcellulose, hydroxypropyl methyl cellulose, and ethyl cellulose) and nanocellulose are being used as strengthening or reinforcing agents in different studies. However, cellulose ethers are chemically modified cellulose while nanocellulose is nano-sized cellulose free from lignin and hemicellulose⁶. The literature also shows that the presence of hydrogen bonds in nanocellulose enhances the material stiffness and postpones the initiation and evolution of damage with a somewhat reduction in the brittleness of the polymer³³. In the earlier reports, rice nanocellulose was evaluated for the *in-vitro* cytotoxicity property by using HeLa and SiHa cell lines and results showed 100% cell viability of HeLa and SiHa cells revealing the non-cytotoxicity of rice nanocellulose³⁹. In this study, the polymeric films were prepared by employing the solvent casting method. In the xanthan gum film, extracted nanocellulose was utilized as reinforcing material, and PEG and fluconazole were used as a plasticizer and antifungal model drug respectively. The films were prepared by drying at 50 °C, as the films do not dry properly at low temperature. Moreover, it is also mentioned in the literature that drying of nanocellulose-based composite films at high temperature (50-100 °C) improves the tensile strength of the films as compared to the films dried at low temperatures⁴⁰. The experimental design was also implemented for getting an optimized batch of the XNF. XF and NF were also prepared by the same process for the comparative study. The diagrammatic representation of the preparation of XNF has been shown in Figure 1.

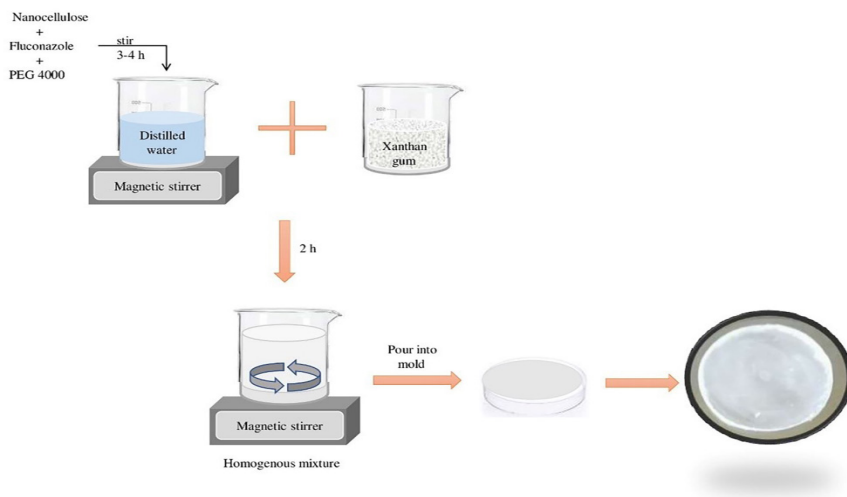


Figure 1. Schematic representation of preparation of fluconazole-loaded xanthan-nanocellulose film

Experimental design

The preliminary trials suggested that the concentration of nanocellulose and PEG highly influenced the drug release property and tensile strength of the composite film. Therefore, in this study, the amount of nanocellulose and PEG were taken as independent variables while drug release (%) and tensile strength (mN) were taken as dependent variables. Table 1 shows the responses obtained from thirteen trial runs generated by the two-factor three-level central composite experimental design.

Table 1. Experimental values of the tensile strength (mN) and cumulative drug release (%) of XNF

Formulations	X ₁ (mg)	X ₂ (mg)	Y ₁ (mN)	Y ₂ (%)
F1	25	15	1100	79.27
F2	25	32.5	1330	76.6
F3	25	50	2100	72.73
F4	62.5	15	2200	63.79
F5	62.5	32.5	2800	57.82
F6	62.5	50	2860	59.46
F7	100	15	2330	50.74
F8	100	32.5	3230	53.7
F9	100	50	4580	46.76
F10	62.5	32.5	2360	57.5
F11	62.5	32.5	2430	59.77
F12	62.5	32.5	2400	58.84
F13	62.5	32.5	2700	65.39

X₁-amount of nanocellulose, X₂- amount of PEG, Y₁-tensile strength (mN), Y₂-cumulative drug release (%)

The responses were fitted into multiple polynomial models using Design Expert® software. It was found that response Y₁ (tensile strength) was best fitted into the two-factor interaction (2FI) model while response Y₂ (% release) was best fitted into the quadratic model without transformation. Equations 3 and 4 showed the relationship between independent variables and response variables.

$$Y_1 = 60.72 - 12.40X_1 - 2.98X_2 - 0.1125X_1X_2 + 3.26X_2^2$$

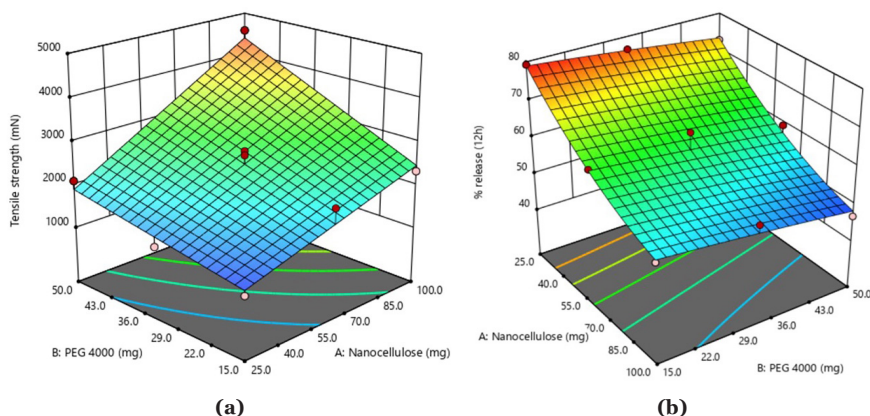
$$Y_2 = 2493.85 + 935.00X_1 + 651.76X_2 + 312.50X_1X_2$$

Table 2 represents the ANOVA results which indicate that polynomial models are significant with a 'non-significant' lack of fit. The R² values of both models were found more than 0.9, depicting the better quality of models, and the difference between adjusted and predicted R² values was found less than 0.2, showing the reasonable difference between actual and predicted values.

Table 2. ANOVA results

Response factor	Model					Lack of fit	
	R ²	Adjusted R ²	Predicted R ²	Adequate precision	C.V.%	F-value	p-value
Y ₁	0.9342	0.9122	0.8105	22.5994	10.15	2.1300	0.2414
Y ₂	0.9546	0.9221	0.8547	17.2934	04.22	0.4772	0.7152

Figure 2 (a) and (b) showed the effect of nanocellulose and PEG on tensile strength and % drug release. As shown in Figure 2a, an increase in tensile strength was observed by increasing the concentration of nanocellulose and PEG. However, the cumulative drug release of formulation decreases as the amount of nanocellulose and PEG increases as depicted in Figure 2b. This may be due to the high surface area and porous nature of nanocellulose²⁵.

**Figure 2.** Response surface plots showing the combined effect of the amount of nanocellulose and PEG on (a) tensile strength and (b) % release.

The numerical optimization tool suggested the optimal concentration of nanocellulose and PEG to formulate an optimized batch of XNF (batch F9). The optimized batch of XNF containing nanocellulose (100 mg), PEG (50 mg), xanthan gum (100 mg), and fluconazole (30 mg) releases the fluconazole (46.76%) in a sustained manner (12 h) with high tensile strength (4580 mN). The batches of XF (xanthan gum – 100 mg, PEG – 50 mg, fluconazole – 30 mg) and NF (nanocellulose – 100 mg, PEG – 50 mg, fluconazole – 30 mg) were also prepared for comparative analysis and further characterized.

Characterization of films

Various physicochemical, structural, and mechanical characterization studies

of XF, NF, and XNF such as thickness, tensile strength, surface pH, swelling index, drug content, and *in vitro* release of films were performed for drug delivery applications.

Physicochemical characterizations

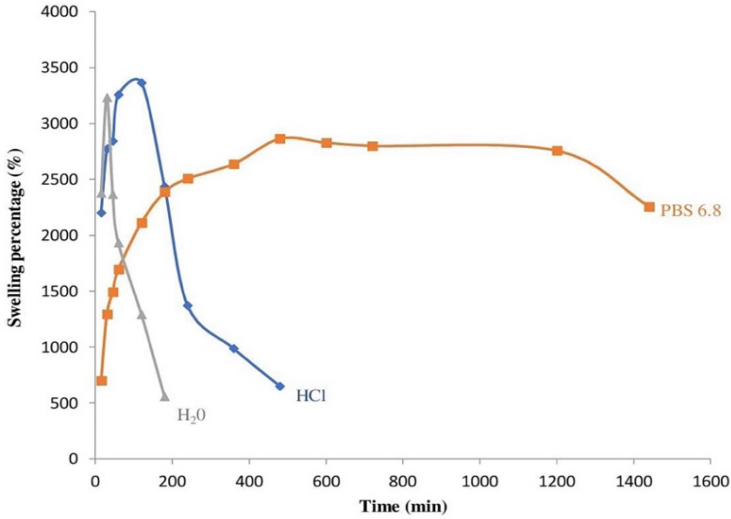
The results of physicochemical characterizations of XF, NF, and XNF are given in Table 3. As shown in Table 3, no significant difference was observed in terms of weight uniformity, thickness, and surface pH. The % moisture content of XF, NF, and XNF was calculated to be $10 \pm 1.5\%$, $1 \pm 0.4\%$, and $2 \pm 0.7\%$ respectively, indicating that reinforcing the xanthan film with nanocellulose reduces the moisture absorption. The average weight of XF, NF, and XNF was found to be in range of 48.9-51.2 mg. The thickness of XF, NF, and XNF was found in the range of 2.12-2.68 mm whereas the surface pH of the polymeric film was found in the range of 6.7-7.0. However, the tensile strength of the nanocellulose-reinforced polymeric film was found more than six-fold in contrast to native xanthan and nanocellulose films which revealed the high mechanical strength of XNF due to the incorporation of nanocellulose.

Table 3. Physicochemical characterization of films

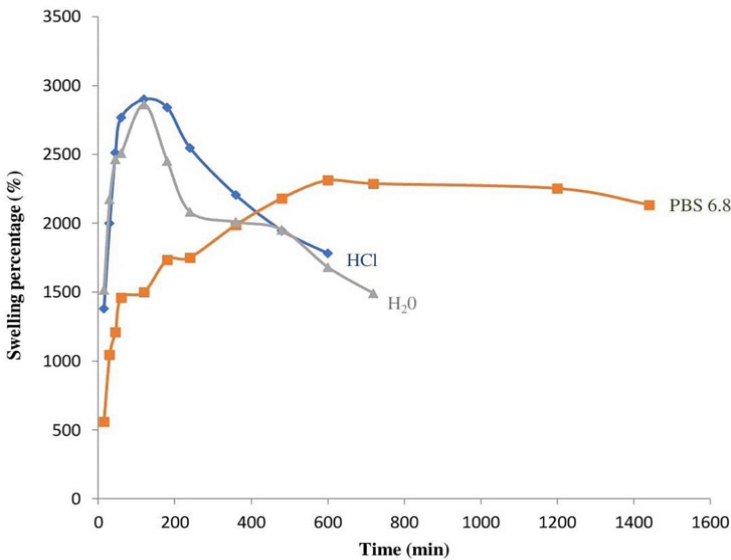
Batch	Moisture content (%)	Average weight (mg)	Thickness (mm)	Tensile strength (mN)	Surface pH
XF	10 ± 1.5	51.2 ± 1.5	2.44 ± 0.2	700 ± 10.1	6.7 ± 0.2
NF	01 ± 0.4	48.9 ± 0.4	2.12 ± 0.1	230 ± 4.5	7.0 ± 0.1
XNF	02 ± 0.7	50.3 ± 0.6	2.68 ± 0.2	4220 ± 15.7	6.9 ± 0.2

Figure 3 (a-c) shows the results of a swelling study of XF, NF, and XNF in 0.1 N HCl (1.2 pH), phosphate buffer solution (6.8 pH), and distilled water. The XF showed faster swelling in water (1 h) and 0.1 N HCl (2 h) with swelling in the range of 3300-3400% and then started to erode while in phosphate buffer pH 6.8, film swelled continuously up to 7 h with swelling of 2800% and then remained constant up to 20 h. After 20 h, XF started to erode in the phosphate buffer. Film erosion may be due to the hydrophilic property of both xanthan gum and nanocellulose which tends to dissolve or disperse in the swelling medium⁴¹. The swelling pattern of NF was found to be similar to XF, with a high percent swelling in water and 0.1 N HCl than phosphate buffer pH 6.8. In water and 0.1 N HCl film swelled up to 2 h and then started to erode but in buffer solution film swelled up to 10 h and then became constant. XNF swelling pattern was similar in all media -water, 0.1 N HCl, and buffer solution with swelling up

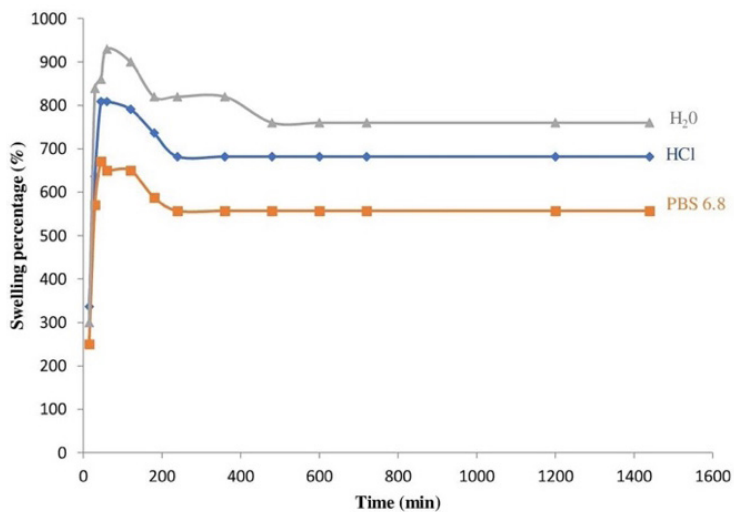
to 1h followed by a slight drop in swelling up to 3 h and then remained stable up to 24 h. The swelling percentage of XNF was higher in water as compared to 0.1 N HCl and buffer solution. Further, it can be observed that reinforcing the xanthan films with nanocellulose limited their erosion.



(a)



(b)

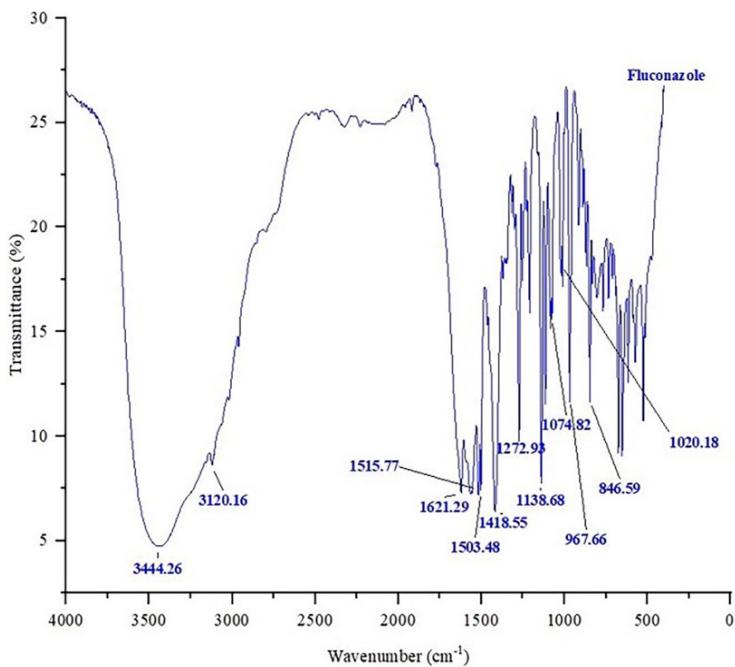


(c)

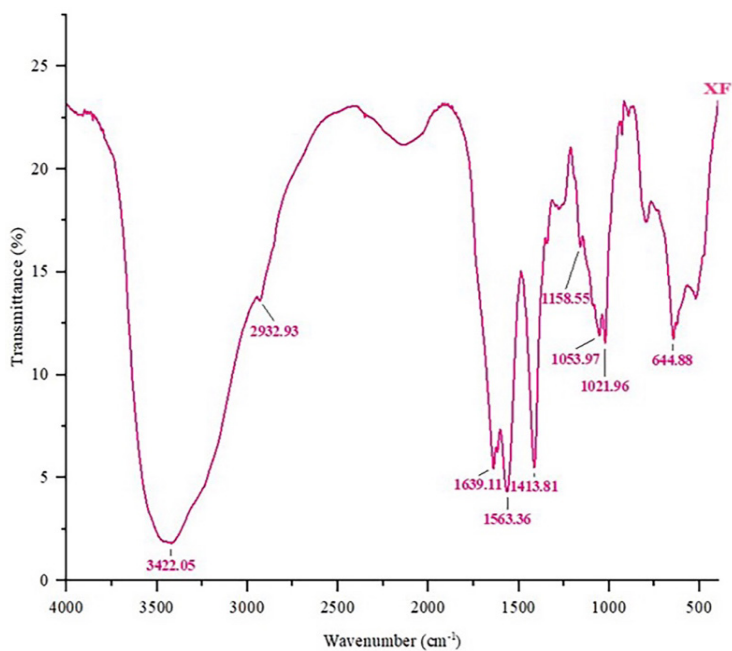
Figure 3. Swelling property of (a) XF, (b) NF, and (c) XNF in distilled water, HCl, and phosphate buffer

FT-IR

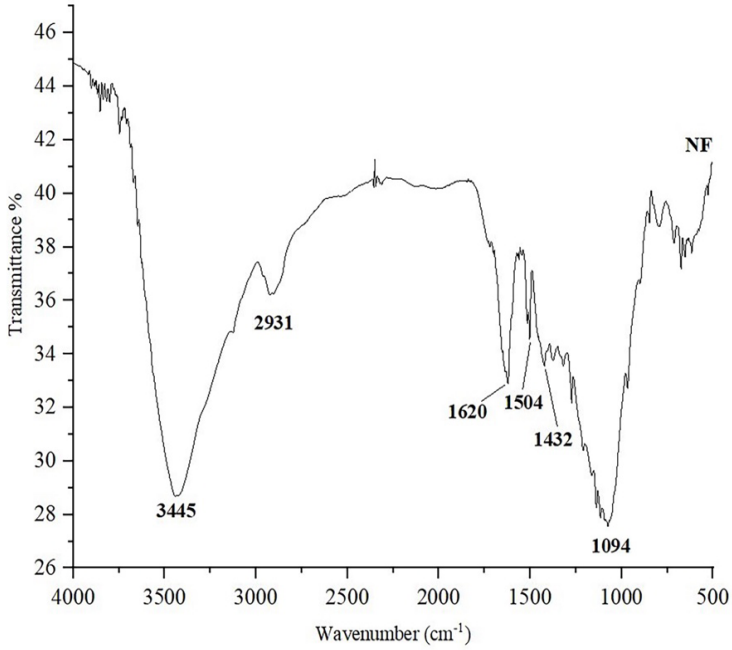
The FT-IR spectra of fluconazole, XF, NF, and XNF have been shown in Figure 4. Fluconazole shows an absorption band at 3444.16 cm^{-1} due to O-H stretching vibrations. Peaks at 1621.29 cm^{-1} and 1515.77 cm^{-1} occurred due to the C=C stretching. The sharp peaks at 1503.48 cm^{-1} and 1418.55 cm^{-1} represented the triazole ring stretching. Peaks at 1272.93 cm^{-1} , 1138.68 cm^{-1} and 1074.82 cm^{-1} exhibited the C-F stretch, triazole ring stretch, and ring bending mode of fluconazole respectively. The peak at 1020.18 cm^{-1} indicated the presence of a C-H aromatic ring. The peaks at 967.66 cm^{-1} and 846.59 cm^{-1} depicted the C-H of the triazole ring present in fluconazole³³. FT-IR spectrum of XNF showed a characteristic peak at 3447.77 cm^{-1} which represents the O-H stretching. The peaks at 1640.15 cm^{-1} , 1566.39 cm^{-1} , and 1415.05 cm^{-1} occurred due to C=O stretching of the carboxylate group, C=O of enols, and -COO stretch respectively. These peaks are also present in XF and NF spectra with slight differences in the peak positions. The peak shown at 1021.18 cm^{-1} at the low depth indicated that fluconazole was incorporated with xanthan gum. A peak at 643.92 cm^{-1} is also associated with -COO stretch^{33,42-43}. The spectrum of XNF confirms the presence of fluconazole and reinforcement with rice nanocellulose.



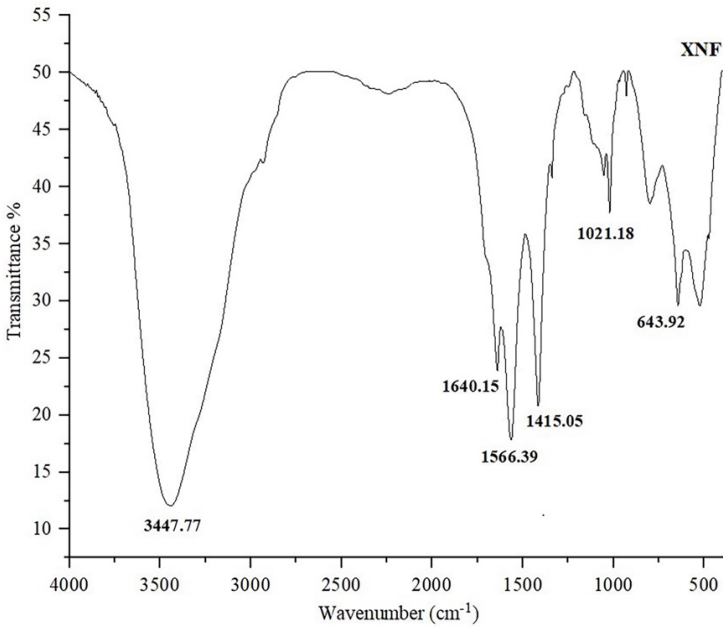
(a)



(b)



(c)

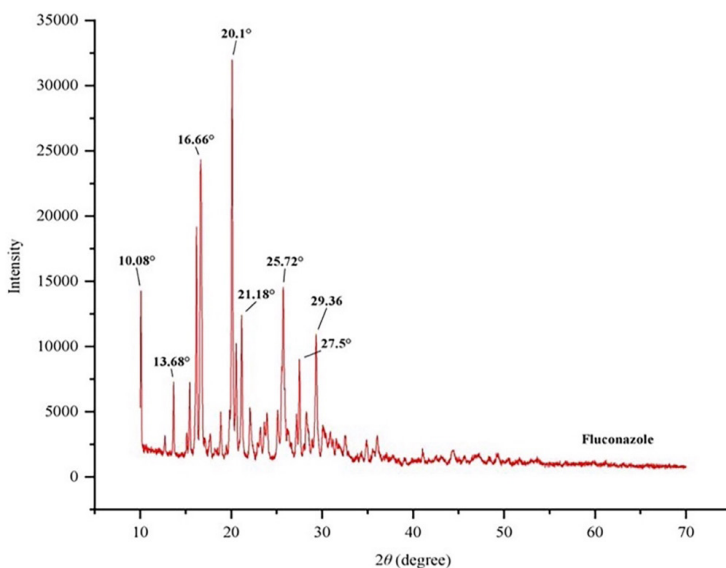


(d)

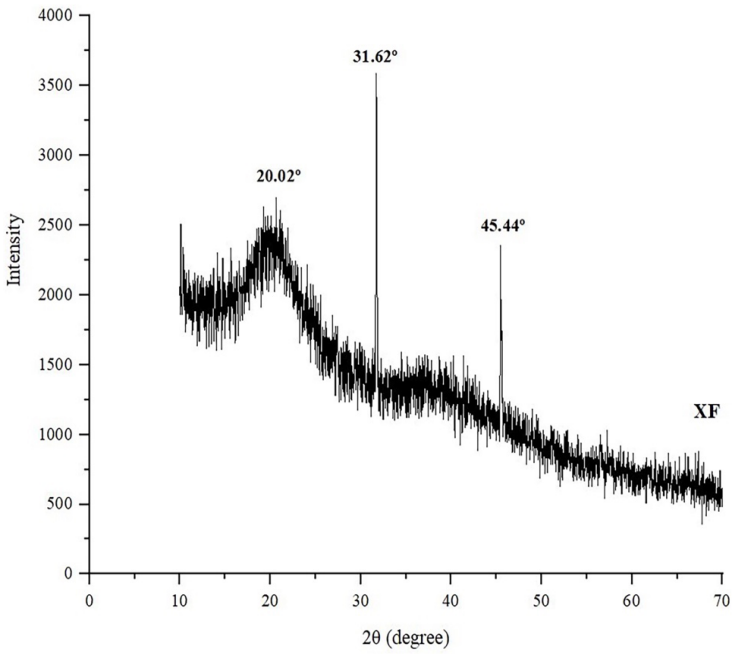
Figure 4. FT-IR spectrum of (a) Fluconazole, (b) XF, (c) NF, and (d) XNF

XRD

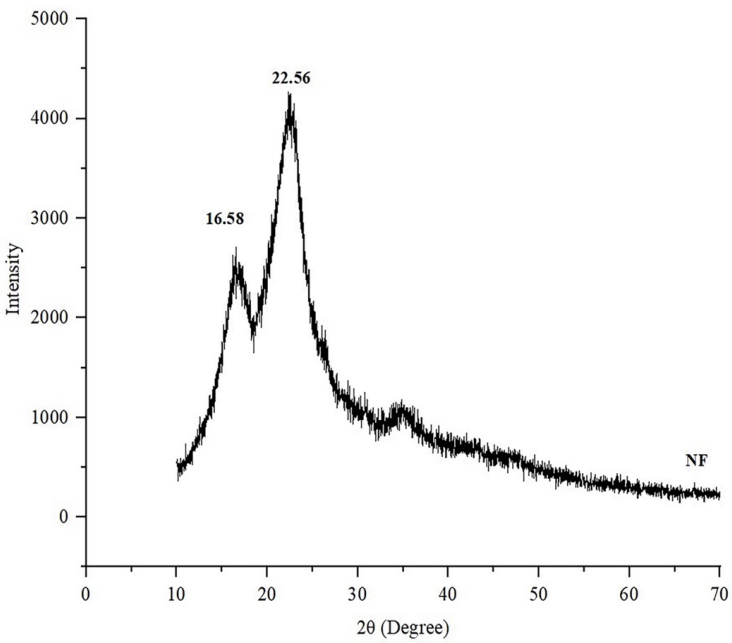
The X-ray diffractogram of fluconazole, XF, NF and XNF has been shown in Figure 5. Fluconazole diffractogram depicted the intense peaks at 2θ values of 10.08° , 13.68° , 16.66° , 20.10° , 21.18° , 25.72° , 29.36° and 27.5° indicating the crystalline nature of fluconazole. The diffractogram of XF showed sharp peaks at 2θ values of 20.02° , 31.62° , and 45.44° and NF exhibited sharp peaks at 16.58° and 22.56° representing that both XF and NF are amorphous in nature. XNF diffractogram presented the peaks at 2θ values of 17.6° , 18.5° , and 22.5° revealing the amorphous nature of the film. Hence, it can be seen that the diffractograms of XF, NF and XNF are showing the amorphous nature and there is no significant difference in their diffraction patterns.



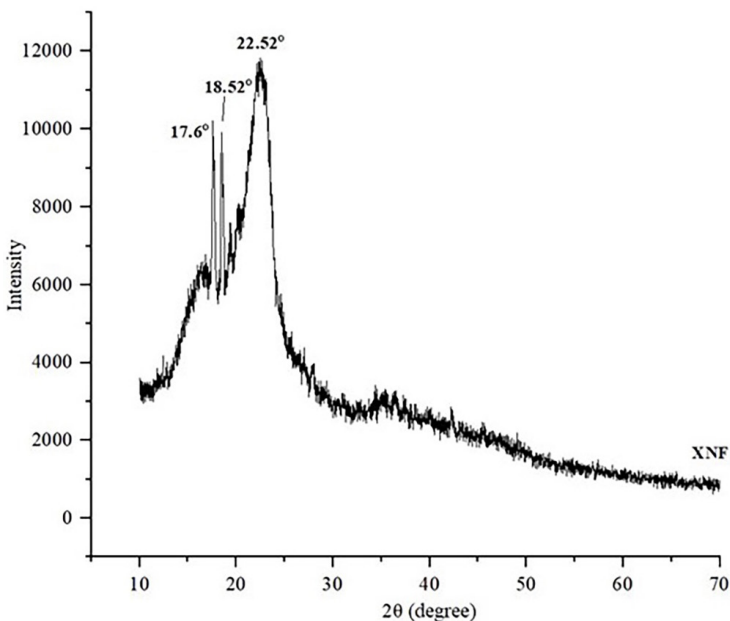
(a)



(b)



(c)



(d)

Figure 5. XRD diffractogram of (a) Fluconazole, (b) XF, (c) NF and (d) XNF

SEM

The scanning electron micrograph of an optimized batch of XNF was captured at 200x. As shown in Figure 6, the fibrous surface of XNF was observed. The cylindrical-shaped nanocellulose fibers embedded in the xanthan gum film were present on the surface of the polymeric film.

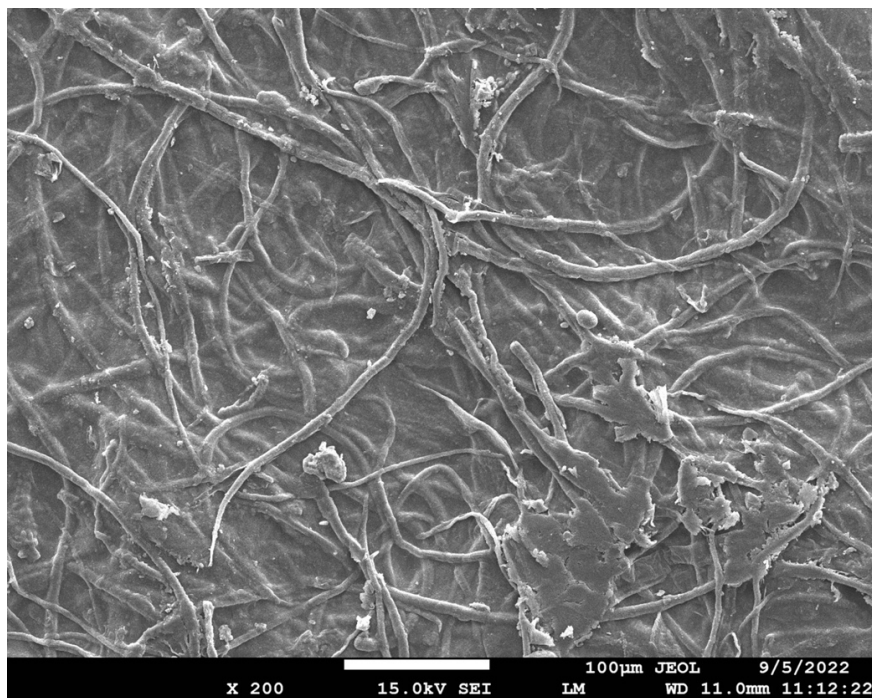


Figure 6. SEM image of XNF

***In vitro* release study**

Initially, the amount of fluconazole drug present in the film was estimated by measuring absorbance using a UV spectrophotometer at wavelength 260 nm. The drug content was calculated and found to be 97.83%, 99.14%, and 102.89% of XF, NF, and XNF respectively. Then, the *in-vitro* release of fluconazole from XF, NF, and XNF was performed up to 24 h in phosphate buffer at pH 6.8. The plot of cumulative release (%) vs time (h) of XF, NF, and XNF is shown in Figure 7. It can be observed that almost all of the fluconazole was released from NF in 8 h, while it took 16 h to release 100% of fluconazole from XF. On the other hand, nanocellulose-reinforced XNF could sustain the release for up to 24 h. It can be concluded that after the reinforcement of nanocellulose in xanthan gum, the release of fluconazole was more sustained compared to native xanthan gum film. The *in vitro* release data of XF, NF, and XNF was also fitted into various kinetics models to recognize the release mechanism of fluconazole (Table 4). The kinetic data analysis of XF, NF, and XNF revealed that the release of fluconazole from XF and NF follows the Higuchi model while XNF follows the zero-order kinetics⁴⁴. The Higuchi model describes the release of less

soluble or very soluble drugs from a solid matrix system through the porosity of the matrix. In the case of XNF, due to its high tensile strength, XNF showed a delay in disintegration and resulted in a very slow drug release. When the release is time-dependent and concentration-independent it means zero-order kinetics has been followed by the formulation. This drug release method is ideal for achieving prolonged pharmacological action. The release exponent, 'n' values of the Korsmeyer-Peppas model indicated that the mechanism of drug release for both XF and NF ($0.5 < n < 0.89$) is anomalous transport while release from XNF ($n > 1$) represents super case II transport⁴⁵⁻⁴⁷. Anomalous transport shows that mechanism of drug release is controlled by swelling and diffusion while super case II transport represents the diffusion and relaxation of polymer chains⁴⁸.

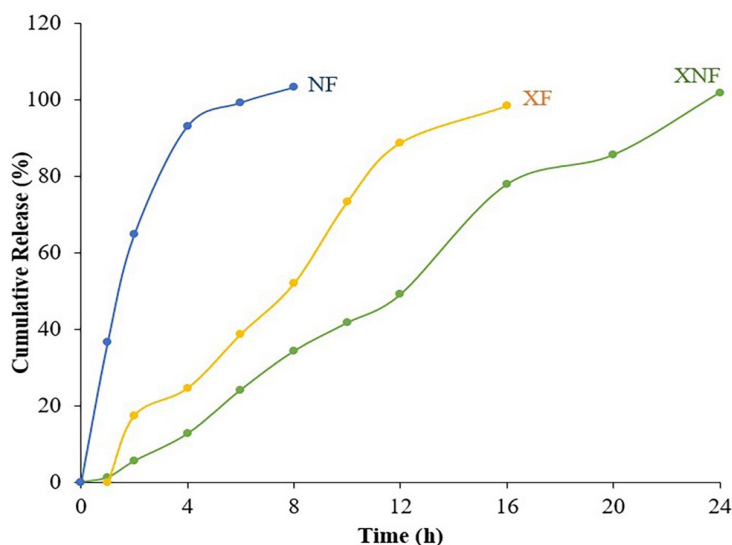


Figure 7. *In-vitro* drug release profile of XF, NF, and XNF

Table 4. Data of kinetic models

Sr. No.	Batch	Zero-order (R ²)	First-order (R ²)	Higuchi (R ²)	Korsmeyer-Peppas	
					(R ²)	n
1.	XF	0.9514	0.8281	0.9623	0.9843	0.7061
2.	NF	0.8118	0.9268	0.9611	0.9284	0.6736
3.	XNF	0.9908	0.9336	0.963	0.982	1.3368

In this study, fluconazole-loaded nanocellulose-reinforced xanthan film was prepared by solvent casting method using nanocellulose as a reinforcing agent, xanthan gum as film-forming polymer, PEG as a plasticizer, and fluconazole as a model drug. The optimization technique, a two-factor three-level central composite experimental design was employed to find out the optimized formulation of the film. Thirteen batches of films were prepared and evaluated for their physical and chemical characteristics. The obtained results revealed that all prepared films had sufficient tensile strength with sustained drug-release properties. The optimized batch (nanocellulose = 100 mg, xanthan gum = 100 mg, PEG = 50 mg, and fluconazole = 30 mg) was selected as the best formulation, and it was further characterized. FT-IR study revealed that no interaction takes place between the drug and other excipients while the XRD study confirmed the amorphous nature of the film. The *in vitro* dissolution study showed a fluconazole release of 100% in 24 h. Xanthan gum and nanocellulose possess mucoadhesive properties. Based on the findings of the present study, it can be concluded that reinforcement of xanthan film with nanocellulose improves the mechanical strength and prolongs the *in-vitro* release of the drug. However, further *ex-vivo* and *in-vivo* studies are needed to explore the potential of fluconazole-loaded nanocellulose-reinforced xanthan films for mucoadhesive or topical drug delivery applications.

STATEMENT OF ETHICS

This study does not require any ethical permission.

CONFLICT OF INTEREST STATEMENT

No conflicts of interest.

AUTHOR CONTRIBUTIONS

All the authors contributed to the study design, and preparation of the manuscript, and all have read and approved the final version. The specific activities of them were Vipin Jain: methodology, acquisition of data, drafting of the manuscript. Rimpay Pahwa and Rashmi Sharma: sample analysis, discussion, data analysis, and paper preparation. Munish Ahuja: design of methodology, planning, data discussion, and mentorship.

FUNDING SOURCES

This research did not receive any specific grant from funding agencies in the public, commercial or not-for-profit sectors.

REFERENCES

1. Meydanju N, Pirsá S, Farzi J. Biodegradable film based on lemon peel powder containing xanthan gum and TiO₂-Ag nanoparticles: Investigation of physicochemical and antibacterial properties. *Polym Testing*, 2022;106(12). Doi: 10.1016/j.polymertesting.2021.107445
2. Shiledar RR, Tagalpallear AA, Kokare CR. Formulation and in vitro evaluation of xanthan gum-based bilayered mucoadhesive buccal patches of zolmitriptan. *Carbohydr Polym*, 2014;101:1234-1242. Doi: 10.1016/j.carbpol.2013.10.072
3. Jadhav M, Pooja D, Adams DJ, Kulhari H. Advances in xanthan gum-based systems for the delivery of therapeutic agents. *Pharmaceutics*, 2023;15(2):1-27. Doi: 10.3390/pharmaceutics15020402
4. Rimpý, R, Ahuja M. In *Polysaccharide-based Biomaterials: Delivery of Therapeutics and Biomedical Applications*. The Royal Society of Chemistry, 2022, pp. 361-396.
5. Zheng M, Chen J, Tan KB, Chen M, Zhu Y. Development of hydroxypropyl methylcellulose film with xanthan gum and its application as an excellent food packaging bio-material in enhancing the shelf life of banana. *Food Chem*, 2022;374. Doi: 10.1016/j.foodchem.2021.131794
6. Wen Q, Wang X, Liu B, Lu L, Zhang X, Swing CJ, et al. Effect of synergism between sodium alginate and xanthan gum on characteristics of composite film and gloss of areca nut coating. *Food Biosci*, 2022;50. Doi: 10.1016/j.fbio.2022.102113
7. Hazirah MN, Isa MI, Sarbon NM. Effect of xanthan gum on the physical and mechanical properties of gelatin-carboxymethyl cellulose film blends. *Food Packag Shelf Life*, 2016;9:55-63. Doi: 10.1016/j.fpsl.2016.05.008
8. Chen J, Zheng M, Tan KB, Lin J, Chen M, Zhu Y. Polyvinyl alcohol/xanthan gum composite film with excellent food packaging, storage and biodegradation capability as potential environmentally-friendly alternative to commercial plastic bag. *Int J Biol Macromol*, 2022;212:402-411. Doi: 10.1016/j.ijbiomac.2022.05.119
9. Zheng M, Zhu Y, Zhuang Y, Tan KB, Chen J. Effects of grape seed extract on the properties of pullulan polysaccharide/xanthan gum active films for apple preservation. *Int J Biol Macromol*, 2023;241. Doi: 10.1016/j.ijbiomac.2023.124617
10. Singh M, Tiwary AK, Kaur G. Investigations on interpolymer complexes of cationic guar gum and xanthan gum for formulation of bioadhesive films. *Res Pharm Sci*, 2010;5(2):79-87.
11. Shipp L, Liu F, Kerai-Varsani L, Okwuosa TC. Buccal films: a review of therapeutic opportunities, formulations & relevant evaluation approaches. *J Control Release*, 2022;352:1071-1092. Doi: 10.1016/j.jconrel.2022.10.058
12. Gil MC, Park SJ, Lee BS, Park C, Lee BJ. Dual thermal stabilizing effects of xanthan gums via glycosylation and hydrogen bonding and in vivo human bioavailability of desmopressin in orodispersible film. *Int J Pharm*. 2023;637. Doi: 10.1016/j.ijpharm.2023.122879
13. Deshkar SS, Mahore JG. Herbal bioactive-based vaginal and rectal drug delivery systems. *Herbal Bioactive-Based Drug Delivery Systems*. Academic Press; 2022. 111-168. Available from: 10.1016/B978-0-12-824385-5.00017-0
14. Dimofte A, Dinu MV, Anghel N, Doroftei F, Spiridon I. Xanthan and alginate-matrix used as transdermal delivery carrier for piroxicam and ketoconazole. *Int J Biol Macromol*, 2022;209:2084-2096. Doi: 10.1016/j.ijbiomac.2022.04.189
15. Singh S, Nwabor OF, Sukri DM, Wunnoo S, Dumjun K, Lethongkam S, et al. Poly (vinyl alcohol) copolymerized with xanthan gum/hypromellose/sodium carboxymethyl cellulose dermal dressings functionalized with biogenic nanostructured materials for antibacterial and

wound healing application. *Int J Biol Macromol*, 2022;216(24):235-250. Doi: 10.1016/j.ijbiomac.2022.06.172

16. Sun B, Zhang M, Shen J, He Z, Fatehi P, Ni Y. Applications of cellulose-based materials in sustained drug delivery systems. *Curr Med Chem*, 2019;26(14):2485-2501. Doi: 10.2174/0929867324666170705143308

17. Pahwa R, Ahuja M. Nanocellulose-gellan cross-linked scaffolds for vaginal delivery of fluconazole. *Int J of Biol Macromol*, 2023;229:668-683. Doi: 10.1016/j.ijbiomac.2022.12.273

18. Aitomäki Y, Oksman K. Reinforcing efficiency of nanocellulose in polymers. *React Funct Polym*, 2014;85:151-156. Doi: 10.1016/j.reactfunctpolym.2014.08.010

19. Jonoobi M, Mathew AP, Oksman K. Producing low-cost cellulose nanofiber from sludge as new source of raw materials. *Ind Crop Prod*, 2012;40:232-238. Doi: 10.1016/j.indcrop.2012.03.018

20. Kargarzadeh H, Mariano M, Huang J, Lin N, Ahmad I, Dufresne A, et al. Recent developments on nanocellulose reinforced polymer nanocomposites: a review. *Polym*, 2017;132:368-393. Doi: 10.1016/j.polymer.2017.09.043

21. Lee KY, Aitomäki Y, Berglund LA, Oksman K, Bismarck A. On the use of nanocellulose as reinforcement in polymer matrix composites. *Comp Sci Technol*, 2014;105:15-27. Doi: 10.1016/j.compscitech.2014.08.032

22. Mahardika M, Amelia D, Syafri E. Applications of nanocellulose and its composites in bio packaging-based starch. *Mater Today*, 2023;74(3):415-418. Doi: 10.1016/j.matpr.2022.11.138

23. Kargarzadeh H, Huang J, Lin N, Ahmad I, Mariano M, Dufresne A, et al. Recent developments in nanocellulose-based biodegradable polymers, thermoplastic polymers, and porous nanocomposites. *Prog Polym Sci*, 2018;87:197-227. Doi: 10.1016/j.progpolymsci.2018.07.008

24. Lu Y, Weng L, Cao X. Biocomposites of plasticized starch reinforced with cellulose crystallites from cottonseed linter. *Macromol Bio Sci*, 2005;5:1101-1107. Doi: 10.1002/mabi.200500094

25. Liu D, Zhong T, Chang PR, Li K, Wu Q. Starch composites reinforced by bamboo cellulose crystals. *Bioresour Technol*, 2010;101(7):2529-2536. Doi: 10.1016/j.biortech.2009.11.058

26. Li Q, Zhou J, Zhang L. Structure and properties of the nanocomposite films of chitosan reinforced with cellulose whiskers. *J Polym Sci Part B*, 2009;47(11):1069-1077. Doi: 10.1002/polb.21711

27. Khan A, Sp Salmieri, Fraschini C, Bouchard J, Riedl B, Lacroix M. Genipin cross-linked nanocomposite films for the immobilization of antimicrobial agent. *ACS Appl Mater Interfaces*, 2014;6(17):15232-15242. Doi: 10.1021/am503564m

28. Huq T, Salmieri S, Khan A, Khan RA, Le Tien C, Riedl B, et al. Nanocrystalline cellulose (NCC) reinforced alginate based biodegradable nanocomposite film. *Carbohydr Polym*, 2012;90(4):1757-1763. Doi: 10.1016/j.carbpol.2012.07.065

29. Mondragon G, Pena-Rodriguez C, Gonzalez A, Eceiza A, Arbelaiz A. Bionanocomposites based on gelatin matrix and nanocellulose. *Eur Polym J*, 2015;62:1-9. Doi: 10.1016/j.eurpolymj.2014.11.003

30. Pereira ALS, do Nascimento DM, Morais JPS, Vasconcelos NF, Feitosa JPA, Brígida AIS, et al. Improvement of polyvinyl alcohol properties by adding nanocrystalline cellulose isolated from banana pseudo stems. *Carbohydr Polym*, 2014;112:165-172. Doi: 10.1016/j.carbpol.2014.05.090

31. Ilyas RA, Azmi A, Nurazzi NM, Atiqah A, Atikah MS, Ibrahim R, et al. Oxygen permeability properties of nanocellulose reinforced biopolymer nanocomposites. *Mater Today Proc*, 2022;52(5):2414-2419. Doi: 10.1016/j.matpr.2021.10.420
32. Feng Z, Xu D, Shao Z, Zhu P, Qiu J, Zhu L. Rice straw cellulose microfiber reinforcing PVA composite film of ultraviolet blocking through pre-cross-linking. *Carbohydr Polym*, 2022;296. Doi: 10.1016/j.carbpol.2022.119886
33. Rimpay, Ahuja M. Fluconazole-loaded TEOS-modified nanocellulose 3D scaffolds—Fabrication, characterization and its application as vaginal drug delivery system. *J Drug Del Sci Technol*, 2022;75. Doi: 10.1016/j.jddst.2022.103646
34. Sharma R, Pahwa R, Ahuja M. Iodine-loaded poly (silicic acid) gellan nanocomposite mucoadhesive film for antibacterial application. *J Appl Polym Sci*, 2021;138(2). Doi: 10.1002/app.49679
35. Shaikh R, Singh TR, Garland MJ, Woolfson AD, Donnelly RF. Mucoadhesive drug delivery systems. *J Pharm Bioallied Sci*, 2011;3(1):89-100. Doi: 10.4103/0975-7406.76478
36. Nair AB, Shah J, Jacob S, Al-Dhubiab BE, Patel V, Sreeharsha N, et al. Development of mucoadhesive buccal film for rizatriptan: in vitro and in vivo evaluation. *Pharmaceutics*, 2021;13(5):1-16. Doi: 10.3390/pharmaceutics13050728
37. Ahuja M, Thakur K, Kumar A. Amylopectin-g-poly (N-vinyl-2-pyrrolidone): synthesis, characterization and in vitro release behavior. *Carbohydr Polym*, 2014;108:127-134. Doi: 10.1016/j.carbpol.2014.03.007
38. Almeahady AM, El-Say KM, Mubarak MA, Alghamdi HA, Somali NA, Sirwi A, et al. Enhancing the antifungal activity and ophthalmic transport of fluconazole from PEGylated polycaprolactone loaded nanoparticles. *Polymers*, 2022;15(1):209. Doi: 10.3390/polym15010209
39. Pahwa R, Ahuja M. Design and Development of fluconazole-loaded nanocellulose-eudragit vaginal drug delivery system. *J Pharm Innov*, 2023;18:1065-1083. Doi: 10.1007/s12247-022-09705-2
40. Zhou L, Wang K, Bian L, Chang T, Zhang C. Improving properties of curdlan/nanocellulose blended film via optimizing drying temperature. *Food Hydrocoll*, 2023;137. Doi: 10.1016/j.foodhyd.2022.108421
41. Baniyasi H, Kimiaei E, Polez RT, Ajdary R, Rojas OJ, Österberg M, et al. High-resolution 3D printing of xanthan gum/nanocellulose bio-inks. *Int J Biol Macromol*, 2022;209:2020-2031. Doi: 10.1016/j.ijbiomac.2022.04.183
42. Zhu L, Feng L, Luo H, Dong RS, Wang MY, Yao G, et al. Characterization of polyvinyl alcohol-nanocellulose composite film and its release effect on tetracycline hydrochloride. *Ind Crops Prod*, 2022;188. Doi: 10.1016/j.indcrop.2022.115723
43. Prado KS, Spinacé MA. Isolation and characterization of cellulose nanocrystals from pineapple crown waste and their potential uses. *Int J Biol Macromol*, 2019;122:410-416. Doi: 10.1016/j.ijbiomac.2018.10.187
44. Qureshi MA, Arshad N, Rasool A, Rizwan M, Rasheed T. Guar gum-based stimuli responsive hydrogels for sustained release of diclofenac sodium. *Int J Biol Macromol*, 2023;250. Doi: 10.1016/j.ijbiomac.2023.126275
45. Verma S, Rimpay, Ahuja M. Carboxymethyl modification of *Cassia obtusifolia* galactomannan and its evaluation as sustained release carrier. *Int J Biol Macromol*, 2020;164:2823-2834. Doi: 10.1016/j.ijbiomac.2020.08.231

46. Costa P, Lobo JM. Modeling and comparison of dissolution profiles. *Eur J Pharm Sci*, 2001;13(2):123-133. Doi: 10.1016/S0928-0987(01)00095-1
47. Bruschi ML. Strategies to modify the drug release from pharmaceutical systems. Woodhead Publishing; 2015. 63-86. Available from: 10.1016/B978-0-08-100092-2.00005-9
48. Karthikeyan M, Deepa MK, Bassim E, Rahna CS, Raj KS. Investigation of kinetic drug release characteristics and in vitro evaluation of sustained-release matrix tablets of a selective COX-2 inhibitor for rheumatic diseases. *J Pharm Innov*, 2021;16:551-557. Doi: 10.1007/s12247-020-09459-9